Open Access

Journal of Energy and Power Technology

LIDSEN Publishing Inc.

Original Research

Stability Analysis of Autonomous Microgrid Operated at Constant-Frequency with the Consideration of Reactive Power Balance

Daming Zhang [1, *], Xiuhui Tang [2]

1. University of New South Wales, Sydney, Australia; E-Mail: daming.zhang@unsw.edu.au
2. Wuhan Institute of Technology, Wuhan, China; E-Mail: 23051101@wit.edu.cn

* **Correspondence:** Daming Zhang; E-Mail: daming.zhang@unsw.edu.au

Academic Editor: Mohammad Jafari

Special Issue: Design and Operation of Microgrids

Journal of Energy and Power Technology
2023, volume 5, issue 4
doi:10.21926/jept.2304039

Received: September 01, 2023
Accepted: November 19, 2023
Published: November 29, 2023

Abstract

Large-scale autonomous microgrids have potential application values as they can increase renewable energy penetration level without compromising the stability of the existing large power systems. Before their widespread implementation, critical issues like stability analysis etc need to be solved. This paper analyses the stability in an autonomous microgrid operated at constant frequency with the consideration of reactive power balance. Difference equations of reactive power for the grid-forming generator are constructed separately from those for the grid-supporting and grid-feeding generators while the difference equations of the real power for all the generators are the same. For the voltage source inverter with its current controlled by proportional resonant controller, at the fundamental frequency, its output current is disentangled from its terminal voltage and is controlled to trace its reference accurately, namely $i_{out} = i_{out}^{*}$. Therefore, each inverter can be modelled as an equivalent current source and the equivalent circuits for d-component and q-component can be separated from each other. Then, the nodal equations in matrix form for the microgrid system can be established readily. With these, the system level state-space equations are built to study the distribution of eigenvalues. By choosing proper coefficients for real power and reactive power reference generations and controller's parameters, one can make all the

eigenvalues falling in the left-hand-side of the complex plane. Therefore, the system is stable. Such a research paves the way for systematically searching good sets of coefficients and controller's parameters which make system operate safely away from unstable region with necessary margin.

Keywords
AC microgrid; constant frequency; eigenvalues; stability; state-space equation

1. Introduction

Power system is now experiencing dynamic and vibrant changes. With the maturity of grid-integrated hydrogen-fuel-cell technology, hydrogen combustion chamber approach, smoothened generation by combining renewable energy harness and grid-scale energy storage, urgency for operating large-scale autonomous microgrids is not very pressing. Nevertheless, such a technology could alleviate the level of monopoly and keep electricity price reasonably affordable. With the backup technology to cope with serious outage or blackout, the operators of large power systems will lead lives with reduced nervousness. Therefore, design and operation of large-scale autonomous microgrids is very relevant and needs to attract more focused research.

The control for operating the autonomous microgrid includes *f*-P and V-Q method, V-P and *f*-Q method, and V-P control method with separate reactive power handling and at constant frequency [1-11]. Each one has pro and cons. In comparison, both *f*-P, V-Q and V-P, *f*-Q methods need to manage both frequency variation and voltage variation while fixed-frequency or constant-frequency method only manages the voltage variation in the system, and the frequency in the system takes a constant value. Therefore, it is easier to operate the microgrid and shows better power quality of frequency.

In the autonomous microgrid operated by each method, stability analysis is indispensable for ensuring its safe operation. Therefore, it is necessary to build state-space equation for the microgrid system under study in order to work out the eigenvalues for stability analysis [12-17]. This is similar to the stability analysis by using eigenvalue approach for the synchronous generators as described in [18, 19]. The method proposed by the authors in [17] for the constant frequency method is suitable for the system with resistive loads and resistance dominant lines. This is not realistic for a practical autonomous microgrid. To cope with the reactive power balance and consider inductive feature of the system, this paper further establishes difference equations for the grid-forming generator, and grid-supporting and grid-feeding generators. The one for the grid-forming generator is different from those for the grid-supporting and grid-feeding generators. For the voltage source inverter with its current controlled by proportional resonant controller, at the fundamental frequency, from the control flow for tracing current, one can verify that the inverter's output current is disentangled from its terminal voltage. To ensure high power quality, the whole microgrid must be designed in such a way that voltages' deviations from the rated value are small under all loading conditions, even under transients due to switch-on or switch-off of loads or faults etc. With this condition satisfied, the output current of each inverter is controlled to trace its reference accurately, namely $i_{out} = i_{out}^*$. Therefore, each inverter can be modelled as an equivalent current source and

the equivalent circuits for d-component and q-component can be separated from each other. Then, the nodal equations in matrix form can be established readily. With these, the system level state-space equations are built to study the distribution of eigenvalues. By choosing proper coefficients for real power and reactive power reference generations and controller's parameters, one can make all the eigenvalues falling in the left-hand-side of the complex plane. Therefore the system is stable.

The remaining contents are arranged as follows: In Section II, construction of state-space equations for the autonomous microgrid is carried out; Section III discusses the potential issues in the autonomous microgrid; Section IV concludes the paper.

2. Construction of State-Space Equation

2.1 Establishment of the Equivalent Circuit

For a practical autonomous microgrid, some buses or nodes are installed with generators while others are not. In the V-P control method with separate reactive power handling and at constant frequency, each voltage source inverter works in current controlled mode and is equivalent to a current source. To build system level equations, it is necessary to process the nodes without equivalent current sources. The first situation is for a no-source node between two other nodes with sources as shown in Figure 1a. For such a case, one can convert Y-connection to Δ-connection. The relationship of the impedances in the two connections in Figures 1a and 1b is shown below.

$$Z_a = \frac{Z_{lm} \cdot Z_{mn} + Z_{lm} \cdot Z_m + Z_m \cdot Z_{mn}}{Z_m} \tag{1}$$

$$Z_b = \frac{Z_{lm} \cdot Z_{mn} + Z_{lm} \cdot Z_m + Z_m \cdot Z_{mn}}{Z_{mn}} \tag{2}$$

$$Z_c = \frac{Z_{lm} \cdot Z_{mn} + Z_{lm} \cdot Z_m + Z_m \cdot Z_{mn}}{Z_{lm}} \tag{3}$$

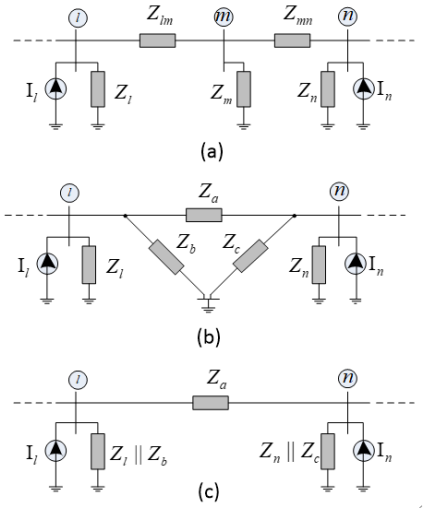

Figure 1 Processing of the nodes without sources: Case 1.

As shown in Figure 1b, an equivalent Δ-connection is obtained for the Y-connection in Figure 1a. Then impedances' combination is done and shown in Figure 1c.

In the second case, the node without a source is at the end of a network or circuit. Then it is combined with its neighboring node with an equivalent current source. Such an approach is shown in Figure 2.

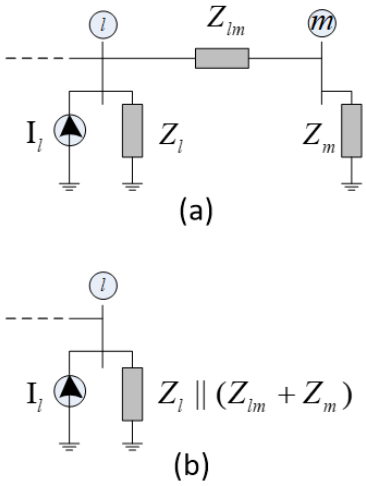

Figure 2 Processing of the nodes without sources: Case 2.

By doing so, one can come to a network, in which each node has an equivalent current source.

2.2 The System under Study and Its Equivalent

Figure 3 shows the single-phase representation of a three-phase autonomous microgrid under study where there are three generators, DG1 being the grid-forming one which is a combination of two inverters (one takes the grid-forming role while the other serves as the reactive power compensator), both DG2 and DG3 being the grid-supporting generators. For a practical autonomous microgrid using V-P control method with separate reactive power handling and at constant frequency, it is necessary to install another back-up grid-forming generator for taking over the main grid-forming generator in case that it becomes faulty including the failure due to the cumulative effect of small negative-sequence currents. To build the system level equations, the circuit in Figure 3a is converted into the one in Figure 3b. By doing so, the modified network or circuit has a source at each node. This is to facilitate the system level state-space equation construction.

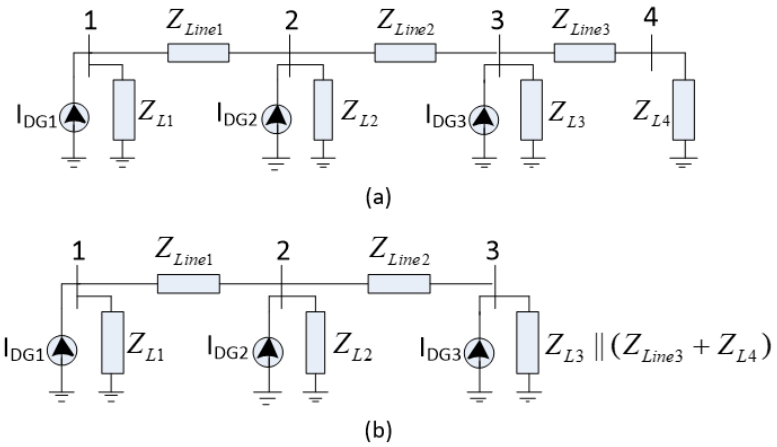

Figure 3 The microgrid under study.

The parameters used for each of the three inverters are shown in Table 1. Selection of proportional resonant controller's parameters can be done by examining four criteria: 1) phase margin of cross-over of open-loop transfer function; 2) resonance suppression for the closed-loop transfer function; 3) step response of the closed-loop transfer function; 4) poles of the closed-loop transfer function [20].

Table 1 Parameters for inverters.

Parameters	Values
L_{1inv}	4.5 mH
C_{inv}	75 µF
L_{2inv}	0.5 mH
$R_{damping}$	1 Ω
fswitching	5 kHz
K_p	0.20
K_i	15.5
K	20.5
$f_{sampling}$	80 kHz
K_{v0}	2000
K_v	1.08
K_{pq}	0.4843

Table 2 shows the loads at each bus while line impedances are given in Table 3.

Table 2 Different loads.

	Load 1	Load 2	Load 3	Load 4
P (kW)	20	40	30	30
Q (kVAr)	10	10	10	10

Table 3 Line impedances.

	Line1	Line2	Line3
R (Ω)	0.6	0.6	0.2
L (mH)	2.5	2.5	1.5

By using the method in [11], one can work out the d-q values of voltages and currents for each bus in Figure 3a. Such values are shown together with other values at subsequent paragraphs.

2.3 Formulation of the Inverter Equations and System Equations

For the neighboring buses, one can establish the following equation in time-domain

$$v_{abc,lm} = R_{lm} i_{lm} + L_{lm} \frac{di_{lm}}{dt} \quad (4)$$

where R_{lm} and L_{lm} are series resistance and inductance between bus *l* and bus *m*.

As $v_{abc,lm} = V_{dq,lm}e^{j\theta}$, $i_{abc,lm} = I_{dq,lm}e^{j\theta}$, one has

$$V_{dq,lm} = (R_{lm} + j\omega L_{lm})I_{dq,lm} \tag{5}$$

For each load,

$$V_{dq,n} = (R_n + j\omega L_n)I_{dq,n} \tag{6}$$

where R_n and L_n are series resistance and inductance of the load at bus *n*.

By building nodal equations for each node or bus, one can assemble and come to the matrix equation as shown below

$$\begin{bmatrix}[I_{dq1}]\\ [I_{dq2}]\\ [I_{dq3}]\end{bmatrix} = \begin{bmatrix}[Y_{dq11}] & [Y_{dq12}] & [Y_{dq13}]\\ [Y_{dq21}] & [Y_{dq22}] & [Y_{dq23}]\\ [Y_{dq31}] & [Y_{dq32}] & [Y_{dq33}]\end{bmatrix}\begin{bmatrix}[V_{dq1}]\\ [V_{dq2}]\\ [V_{dq3}]\end{bmatrix} \tag{7a}$$

or simply

$$[I_{dqT}] = [Y_s][V_{dqT}] \tag{7b}$$

where

$[I_{dqj}] = \begin{bmatrix}I_{dj}\\ I_{qj}\end{bmatrix}$, with I_{dj} and I_{qj} being the d-q components of the equivalent current source at each bus, *j* = 1, 2, 3.

$[V_{dqj}] = \begin{bmatrix}V_{dj}\\ V_{qj}\end{bmatrix}$, with V_{dj} and V_{qj} being the d-q components of the voltage at each bus, *j* = 1, 2, 3.

$[Y_{dqjj}] = \begin{bmatrix}G_j & -B_j\\ B_j & G_j\end{bmatrix}$, *j* = 1, 2, 3.

$[Y_{dqij}] = \begin{bmatrix}G_{ij} & -B_{ij}\\ B_{ij} & G_{ij}\end{bmatrix}$,. *i*= 1, 2, 3, *j* = 1, 2, 3, $i \neq j$.

$G_j + jB_j = \sum(\text{All admittances at bus } j)$, *j* = 1, 2, 3.

$G_{ij} + jB_{ij} = -\sum(\text{Admittances of each branch between bus } i \text{ and bus } j)$, *i*= 1, 2, 3, *j* = 1, 2, 3, $i \neq j$.

From $[I_{dqT}] = [Y_s][V_{dqT}]$, one has

$$[\Delta I_{dqT}] = [Y_s][\Delta V_{dqT}] \tag{8}$$

$$[\Delta \dot{I}_{dqT}] = [Y_s][\Delta \dot{V}_{dqT}] \tag{9a}$$

or simply

$$[\Delta \dot{I}] = [Y_s][\Delta \dot{V}] \tag{9b}$$

For the grid-supporting and grid-feeding generators [10, 11], one has

$$P_{ref} = P_{ref0} + K_{v0} \cdot (K_v \cdot V_{ref} - V_m) \tag{10}$$

$$Q_{ref} = K_{pq}P_{ref} \tag{11}$$

$$\Delta P = -K'_{v0}\Delta V \tag{12}$$

$$\Delta Q = -K_{pq}K'_{v0}\Delta V \tag{13}$$

where $K'_{v0} = K_{v0}/3$ as equation (10) is for three phase but the following formulation is for single phase. K_{v0} is chosen to be 2000 in Table 1. This level of value can cope with temporary unbalanced loads without losing stability. For very balanced loads, K_{v0} can be quite high and it could be as high as 5000. Correspondingly, K_i in the proportional resonant controller should be reduced and it could be as low as 5 or even less. Although greater K_{v0} results in smaller deviation of the inverter's terminal voltage from its targeted value, it could lead to instability when the inverter currents contain un-negligible negative-sequence components.

From $V = \sqrt{V_d^2 + V_q^2}$, one has

$$\Delta V = \frac{V_d\Delta V_d + V_q\Delta V_q}{\sqrt{V_d^2 + V_q^2}} \tag{14}$$

Then

$$\begin{bmatrix}\Delta P\\ \Delta Q\end{bmatrix} = \begin{bmatrix}\frac{-K'_{v0}V_d}{\sqrt{V_d^2 + V_q^2}} & \frac{-K'_{v0}V_q}{\sqrt{V_d^2 + V_q^2}}\\ \frac{-K_{pq}K'_{v0}V_d}{\sqrt{V_d^2 + V_q^2}} & \frac{-K_{pq}K'_{v0}V_q}{\sqrt{V_d^2 + V_q^2}}\end{bmatrix}\begin{bmatrix}\Delta V_d\\ \Delta V_q\end{bmatrix} \tag{15}$$

For the grid-forming generator, one has

$$Q_1 = -Q_2 - Q_3 + Q_{L12} + Q_{L23} + \sum Q_{Loadj} \tag{16}$$

where

$Q_{L12} = |V_1 - V_2|^2 \cdot \frac{X_{12}}{R_{12}^2+X_{12}^2}$, $Q_{L23} = |V_2 - V_3|^2 \cdot \frac{X_{23}}{R_{23}^2+X_{23}^2}$, $Q_{Loadj} = V_j^2 \cdot \frac{X_j}{R_j^2+X_j^2}$, j = 1, 2, 3.

Then one can derive and come to

$$\Delta Q_1 = -\Delta Q_2 - \Delta Q_3 + \Delta Q_{L12} + \Delta Q_{L23} + \sum \Delta Q_{Loadj} \tag{17}$$

where

$\Delta Q_{L12} = C_{12} \cdot (\Delta V_1 - \Delta V_2)$, $\Delta Q_{L23} = C_{23} \cdot (\Delta V_2 - \Delta V_3)$ with $C_{12} = \frac{(V_1-V_2)^2}{|V_1-V_2|^2} \cdot 2(V_1 - V_2)$, $C_{23} = \frac{(V_2-V_3)^2}{|V_2-V_3|^2} \cdot 2(V_2 - V_3)$, $\Delta V_j = \frac{V_{dj}\Delta V_d + V_{qj}\Delta V_q}{\sqrt{V_{dj}^2+V_{qj}^2}}$, and $\Delta Q_{Loadj} = C_{jj} \cdot \Delta V_j$with $C_{jj} = \frac{{V_j}^2}{|V_j|^2} \cdot 2V_j \cdot \frac{X_j}{R_j^2+X_j^2}$, j = 1, 2, 3.

Then

$$\begin{bmatrix}\Delta P_1\\ \Delta Q_1\\ \Delta P_2\\ \Delta Q_2\\ \Delta P_3\\ \Delta Q_3\end{bmatrix}=\begin{bmatrix}R_{11} & R_{12} & 0 & 0 & 0 & 0\\ R_{21} & R_{22} & R_{23} & R_{24} & R_{25} & R_{26}\\ 0 & 0 & R_{33} & R_{34} & 0 & 0\\ 0 & 0 & R_{43} & R_{44} & 0 & 0\\ 0 & 0 & 0 & 0 & R_{55} & R_{56}\\ 0 & 0 & 0 & 0 & R_{65} & R_{66}\end{bmatrix}\begin{bmatrix}\Delta V_{d1}\\ \Delta V_{q1}\\ \Delta V_{d2}\\ \Delta V_{q2}\\ \Delta V_{d3}\\ \Delta V_{q3}\end{bmatrix} \tag{18a}$$

or

$$[\Delta S_T]=[RR]\left[\Delta V_{dqT}\right] \tag{18b}$$

where

$$RR=\begin{bmatrix}R_{11} & R_{12} & 0 & 0 & 0 & 0\\ R_{21} & R_{22} & R_{23} & R_{24} & R_{25} & R_{26}\\ 0 & 0 & R_{33} & R_{34} & 0 & 0\\ 0 & 0 & R_{43} & R_{44} & 0 & 0\\ 0 & 0 & 0 & 0 & R_{55} & R_{56}\\ 0 & 0 & 0 & 0 & R_{65} & R_{66}\end{bmatrix}$$

with

$R_{11}=\frac{-K'_{v0}V_{d1}}{\sqrt{V_{d1}^2+V_{q1}^2}}$, $R_{12}=\frac{-K'_{v0}V_{q1}}{\sqrt{V_{d1}^2+V_{q1}^2}}$, $R_{21}=(C_{11}+C_{12})\cdot\frac{V_{d1}}{\sqrt{V_{d1}^2+V_{q1}^2}}$, $R_{22}=(C_{11}+C_{12})\cdot\frac{V_{q1}}{\sqrt{V_{d1}^2+V_{q1}^2}}$,

$R_{23}=\left(K_{pq2}\cdot K'_{v02}-C_{12}+C_{22}+C_{23}\right)\cdot\frac{V_{d2}}{\sqrt{V_{d2}^2+V_{q2}^2}}$, $R_{24}=\left(K_{pq2}\cdot K'_{v02}-C_{12}+C_{22}+C_{23}\right)\cdot\frac{V_{q2}}{\sqrt{V_{d2}^2+V_{q2}^2}}$,

$R_{25}=\left(K_{pq3}\cdot K'_{v03}-C_{23}+C_{33}\right)\cdot\frac{V_{d3}}{\sqrt{V_{d3}^2+V_{q3}^2}}$, $R_{26}=\left(K_{pq3}\cdot K'_{v03}-C_{23}+C_{33}\right)\cdot\frac{V_{q3}}{\sqrt{V_{d3}^2+V_{q3}^2}}$,

$R_{33}=\frac{-K'_{v02}V_{d2}}{\sqrt{V_{d2}^2+V_{q2}^2}}$, $R_{34}=\frac{-K'_{v02}V_{q2}}{\sqrt{V_{d2}^2+V_{q2}^2}}$, $R_{43}=\frac{-K_{pq2}K'_{v02}V_{d2}}{\sqrt{V_{d2}^2+V_{q2}^2}}$, $R_{45}=\frac{-K_{pq2}K'_{v02}V_{q2}}{\sqrt{V_{d2}^2+V_{q2}^2}}$,

$R_{55}=\frac{-K'_{v03}V_{d3}}{\sqrt{V_{d3}^2+V_{q3}^2}}$, $R_{56}=\frac{-K'_{v03}V_{q3}}{\sqrt{V_{d3}^2+V_{q3}^2}}$, $R_{65}=\frac{-K_{pq3}K'_{v03}V_{d3}}{\sqrt{V_{d3}^2+V_{q3}^2}}$, $R_{66}=\frac{-K_{pq3}K'_{v03}V_{q3}}{\sqrt{V_{d3}^2+V_{q3}^2}}$.

For each of the grid-forming generator, grid-supporting and grid-feeding generators, from $P_{ref}=P_{ref0}+K_{v0}\cdot(K_v\cdot V_{ref}-V_m)$, one can come to

$$\Delta V=-\frac{1}{K'_{v0}}\cdot\left(\frac{\omega_f}{s+\omega_f}\Delta P\right) \tag{19}$$

where ω_f is chosen to be $2\pi\times 10$ and it is to consider the delay for the outer power control loop.

Then

$$\dot{\Delta V}=-\omega_f\Delta V-\frac{\omega_f}{K'_{v0}}\cdot\Delta P \tag{20}$$

$$\dot{\Delta V_d}=\frac{b}{bc-ad}\dot{\Delta V} \tag{21}$$

$$\dot{\Delta V_q} = -\frac{a}{bc-ad}\dot{\Delta V} \tag{22}$$

where $a = \frac{-V_q}{V_d^2+V_q^2}$, $b = \frac{V_d}{V_d^2+V_q^2}$, $c = \frac{V_d}{\sqrt{V_d^2+V_q^2}}$, $d = \frac{V_q}{\sqrt{V_d^2+V_q^2}}$.

In matrix form,

$$\left[\dot{\Delta V_{dqj}}\right] = [M_j]\left[\Delta V_{dqj}\right] + [C_j][\Delta S_j] \tag{23}$$

where

$$\left[\dot{\Delta V_{dqj}}\right] = \begin{bmatrix}\dot{\Delta V_{dj}}\\ \dot{\Delta V_{qj}}\end{bmatrix}, [M_j] = \begin{bmatrix}-\frac{bc\omega_f}{bc-ad} & -\frac{bd\omega_f}{bc-ad}\\ \frac{ac\omega_f}{bc-ad} & \frac{ad\omega_f}{bc-ad}\end{bmatrix}, [C_j] = \begin{bmatrix}-\frac{b\omega_f}{(bc-ad)\cdot K'_{v0j}} & 0\\ \frac{a\omega_f}{(bc-ad)\cdot K'_{v0j}} & 0\end{bmatrix}, j = 1, 2, 3.$$

As $P + jQ = (V_d + jV_q)\cdot(I_d + jI_q)^*$, one can derive and come to

$$[\Delta S_j] = \left[V_{dqj}\right]\left[\Delta I_{dqj}\right] + \left[I_{dqj}\right]\left[\Delta V_{dqj}\right] \tag{24}$$

where

$[\Delta S_j] = \begin{bmatrix}\Delta P_j\\ \Delta Q_j\end{bmatrix}$, $[V_{dqj}] = \begin{bmatrix}V_{dj} & V_{qj}\\ V_{qj} & -V_{dj}\end{bmatrix}$, $[\Delta I_{dqj}] = \begin{bmatrix}\Delta I_{dj}\\ \Delta I_{qj}\end{bmatrix}$, $[I_{dqj}] = \begin{bmatrix}I_{dj} & I_{qj}\\ -I_{qj} & I_{dj}\end{bmatrix}$, $[\Delta V_{dqj}] = \begin{bmatrix}\Delta V_{dj}\\ \Delta V_{qj}\end{bmatrix}$, $j = 1, 2, 3$.

By assembling the equations for each individual node, one can come to the system equation

$$[\Delta S_T] = \left[V_{dqT}\right]\cdot\left[\Delta I_{dqT}\right] + \left[I_{dqT}\right]\cdot\left[\Delta V_{dqT}\right] \tag{25}$$

where

$$[\Delta S_T] = \begin{bmatrix}[\Delta S_1]\\ [\Delta S_2]\\ [\Delta S_3]\end{bmatrix}, [V_{dqT}] = \begin{bmatrix}[V_{dq1}] & [0] & [0]\\ [0] & [V_{dq2}] & [0]\\ [0] & [0] & [V_{dq3}]\end{bmatrix}, [\Delta I_{dqT}] = \begin{bmatrix}[\Delta I_{dq1}]\\ [\Delta I_{dq2}]\\ [\Delta I_{dq3}]\end{bmatrix}, [\Delta V_{dqT}] = \begin{bmatrix}[\Delta V_{dq1}]\\ [\Delta V_{dq2}]\\ [\Delta V_{dq3}]\end{bmatrix},$$

$$[I_{dqT}] = \begin{bmatrix}[I_{dq1}] & [0] & [0]\\ [0] & [I_{dq2}] & [0]\\ [0] & [0] & [I_{dq3}]\end{bmatrix}.$$

From the derivation given in [17], one has the following equation

$$\left[\dot{\Delta V_{dqT}}\right] = [M_T]\left[\Delta V_{dq}\right] + [C_T][\Delta S_T] \tag{26}$$

where

$$[M_T] = \begin{bmatrix}[M_1] & [0] & [0]\\ [0] & [M_2] & [0]\\ [0] & [0] & [M_3]\end{bmatrix}, [C_T] = \begin{bmatrix}[C_1] & [0] & [0]\\ [0] & [C_2] & [0]\\ [0] & [0] & [C_3]\end{bmatrix}.$$

As $[\Delta S_T] = [V_{dqT}]\cdot[\Delta I_{dqT}] + [I_{dqT}]\cdot[\Delta V_{dqT}]$, and $[\Delta S_T] = [RR][\Delta V_{dqT}]$, one can come to

$$[\Delta S_T] = [RR]\left[\Delta V_{dqT}\right] = \left[V_{dqT}\right]\cdot\left[\Delta I_{dqT}\right] + \left[I_{dqT}\right]\cdot\left[\Delta V_{dqT}\right] \tag{27a}$$

$$\left[\Delta V_{dqT}\right] = \left([RR] - \left[I_{dqT}\right]\right)^{-1}\left[V_{dqT}\right] \cdot \left[\Delta I_{dqT}\right] \tag{27b}$$

From Eqns. (25) and (26), one can come to

$$\left[\Delta \dot{V}_{dqT}\right] = \left([M_T] + [C_T] \cdot \left[I_{dqT}\right]\right) \cdot \left[\Delta V_{dq}\right] + [C_T] \cdot \left[V_{dqT}\right] \cdot \left[\Delta I_{dqT}\right] \tag{28}$$

From Eqns. (9a) and (28), then

$$\left[\Delta \dot{V}_{dqT}\right] = [Y_s]^{-1}\left[\Delta \dot{I}_{dqT}\right] = \left([M_T] + [C_T] \cdot \left[I_{dqT}\right]\right) \cdot \left[\Delta V_{dq}\right] + [C_T] \cdot \left[V_{dqT}\right] \cdot \left[\Delta I_{dqT}\right] \tag{29}$$

From (27b) and (29), one can derive and come to

$$\left[\Delta \dot{I}_{dqT}\right] = [\mathrm{M_{total}}] \cdot \left[\Delta I_{dqT}\right] \tag{30}$$

where

$$\mathrm{M_{total}} = [Y_s] \cdot \left\{\left([M_T] + [C_T] \cdot \left[I_{dqT}\right]\right) \cdot \left([RR] - \left[I_{dqT}\right]\right)^{-1}\left[V_{dqT}\right] + [C_T] \cdot \left[V_{dqT}\right]\right\} \tag{31}$$

2.4 Results

For the system with the parameters as shown in Tables 1, 2 and 3, the steady-state d-q values of voltages and currents at each bus are shown in Table 4. These results were obtained by using the method as described in [10, 11, 20]. They can also be obtained by using multi-rate modeling in Matlab/Simulink, namely, T_s is set in POWERGUI for the system modeling; n_1*T_s is used for data acquisition and processing to produce the reference voltages; n_2*T_s is used for the reference voltages updating in comparison with triangular waveform to produce on and off gating signals.

Table 4 d-q values under steady state.

Steady-state values	Bus 1	Bus 2	Bus 3	Bus 4
V_d (V)	237.19	239.254	234.72	221.02
V_q (V)	49.05	27.503	15.524	0
I_d (A)	46.346	53.334	67.606	0
I_q (A)	6.845	-18.600	-27.383	0

The matrix $\mathrm{M_{total}}$ for the system under study with the chosen coefficients and controller's parameters is given below

$$\mathrm{M_{total}} = \begin{bmatrix} -53583 + j99 & -8219 + j15 & -9362 - j126 & -15527 + j44 & -1329 - j59 & 27 + j \\ -13729 - j78 & -5079 - j11 & 9452 + j99 & 16207 - j35 & 1040 + j46 & -21 - j \\ -2300 - j85 & -2934 - j13 & -36896 + j109 & 30241 - j38 & -3407 + j51 & -3121 - j \\ 1995 + j74 & 2545 + j11 & -25002 - j94 & -34171 + j33 & 4213 - j44 & 3563 + j \\ 0 & 0 & -8325 & -15889 & -48221 & 1035 \\ 0 & 0 & 8640 & 16491 & -9535 & -4252 \end{bmatrix}$$

The imaginary parts of the elements in $\mathrm{M_{total}}$ are due to the derivatives of absolute of a function using $|f(x)|' = \{f(x)/|f(x)|\} \cdot f'(x)$, which are negligible.

The corresponding six eigenvalues are shown in Table 5. One can see that the real part of each of them is negative and they fall in the left-hand side of a complex plane. Therefore the chosen coefficients and controller's parameters make the system stable.

Table 5 Six eigenvalues of the system.

		1	2	3	4	5	6
Eigenvalues	Real part	-35628	-35553	-57319	-49616	-3660	-425
	Imaginary part	30374	-30233	26	63	0	0

Tables 6 through 9 show more cases, from which one can see that both $K_{v0,j}$, $K_{pq,j}$ and $K_{v,j}$ influence the location of eigenvalues. For either case, the system is stable. Besides the influence brought by $K_{v0,j}$, $K_{pq,j}$ and $K_{v,j}$, the stability is also influenced by the connection impedances between inverters. To avoid drastic change of inverters' terminal voltages due to load changes and even instability, one needs to keep the rated current times the connection impedance low. For a practical microgrid system, the connection impedances as given in Table 3 at 240 V (phase) or 415 V (line-line) can be reduced.

Table 6 Values of $K_{v0,j}$, $K_{pq,j}$ and $K_{v,j}$.

	K_{v01}	K_{v02}	K_{v03}	K_{pq1}	K_{pq2}	K_{pq3}	$K_{v,j\ (j = 1, 2, 3)}$
Case A	1250	1450	1750	0.45	0.42	0.41	1.08
Case B	2200	2400	2100	0.41	0.46	0.46	1.08
Case C	2750	2800	3000	0.35	0.40	0.39	1.08

Table 7 Six eigenvalues for cases in Table 6.

Eigenvalues		1	2	3	4	5	6
Case A	Real part	-32871	-33335	-54507	-44823	-6818	-660
	Imaginary part	27654	-28395	-60	-70	5	1
Case B	Real part	-36937	-37098	-58521	-49760	-4565	-539
	Imaginary part	29426	-29677	-37	-61	1	1
Case C	Real part	-39449	-38786	-60617	-49017	-7995	-554
	Imaginary part	-28152	27338	-37	103	7	0

Table 8 Values of $K_{v0,j}$, $K_{pq,j}$ and $K_{v,j}$.

	K_{v01}	K_{v02}	K_{v03}	K_{pq1}	K_{pq2}	K_{pq3}	K_{v1}	K_{v2}	K_{v3}
Case D	2750	2800	3000	0.35	0.40	0.39	1.20	1.15	1.21
Case E	2750	2800	3000	0.35	0.40	0.39	1.32	1.24	1.35

Table 9 Six eigenvalues for cases in Table 8.

Eigenvalues		1	2	3	4	5	6
Case D	Real part	-44330	-72135	-45096	-52312	-10810	-616
	Imaginary part	32482	112	-33583	333	19	1

Case E	Real part	-51950	-85006	-51041	-56925	-13435	-674
	Imaginary part	-40049	334	38538	642	26	1

The method developed in the paper is also suitable for the application of other voltage levels.

The above analysis can be modified to suit single-phase autonomous microgrid application. Instead of using d-q frame, one can use x-y components of the complex numbers for the voltages and currents to carry out analysis, e.g. $V_1 = V_{1x} + jV_{1y}$. Similarly, the control methods for three-phase microgrids in [9-11, 20] are suitable for single-phase ones.

3. Discussions

The above analysis is valid for autonomous microgrid systems with balanced loads or equivalently balanced loads. For practical load groups, there are both three-phase and single-phase ones which result in unbalance of the load currents. The currents seen by the inverters need to be as balanced as possible, ideally only containing positive-sequence components. One solution is to add the negative-sequence current compensation at the load side and also use delta-wye connected three-phase transformer to block zero-sequence current [10, 11]. Furthermore, transposition of transmission lines is necessary to increase balance level, even if the line is short. Load-side negative-sequence current compensation may be insufficient. When necessary, one can use a 50 Hz step-down transformer installed at the side of the grid-forming generator with its secondary side in wye connection. Then three single-phase converters can be installed at the secondary side of the transformer to fulfill a small negative-sequence current compensation. To make the control easier, it is good to output a fixed negative-sequence current at one time from the compensator and adjust it to a new value when necessary. In recent simulation study, it is found that by using notch-filter based bandpass filter to remove noise in the current flowing through the shunt capacitor in the inverter's LCL filter with relatively large shunt capacitance and using the second-order Butterworth low-pass filter (with a cut-off frequency around 1 kHz when the switching frequency is chosen to be 5 kHz) to remove high frequency noise in the measured grid-side current [10, 11, 20], with temporary negative-sequence load currents, even at a high proportion level compared with the positive-sequence current, the system still can keep on running. Nevertheless, the voltage waveform becomes distorted and there exists negative-sequence voltage. After the negative-sequence component in the current is gone, the proportional resonant controller with the digital filters can restore the balance of the microgrid system. Then the voltages only contain positive-sequence components.

The higher the ratio of the inverters' terminal voltage to the load voltage, the smaller negative-sequence current experienced by them. Therefore, higher voltages at the inverters' terminals are necessary. To fulfill this purpose, one needs to use IGBT or other switches with higher voltage ratings. Currently in the market the available IGBTs have the voltage ratings as high as 6.5kV and the current rating as high as several thousand amperes. One source of such products is from DYNEX. By using these switches and the circuit topologies as shown in [10, 11], the impact by the negative-sequence current is reduced.

Besides high current IGBT to form one-stage DC/AC converters in the autonomous microgrid, one may also use the multi-stage circuit as shown in Figure 4 where each shunt capacitor comes with a passive damping resistor.

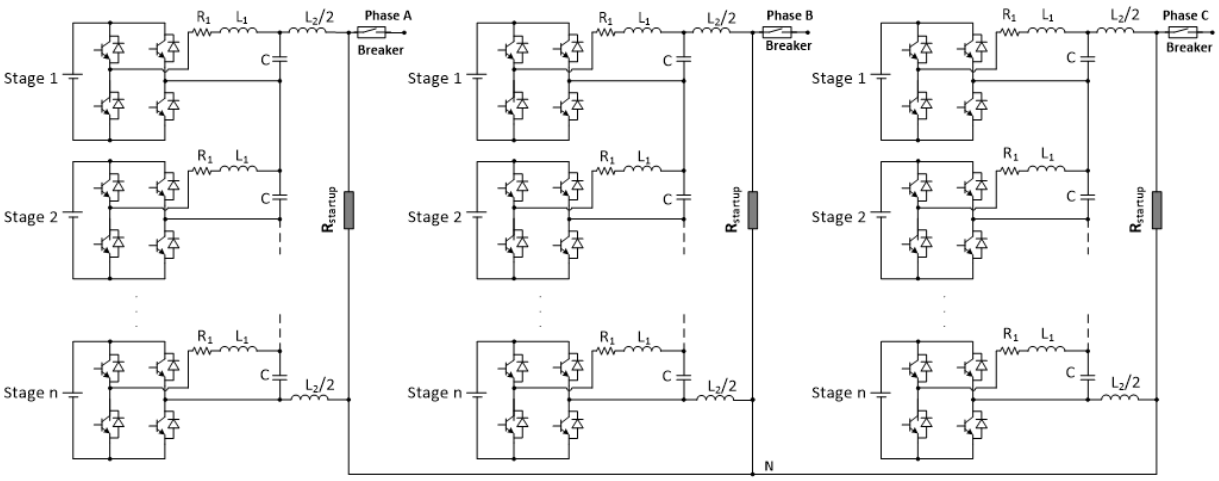

Figure 4 Three-phase inverters with multiple stages.

The equivalent DC sources for each stage in Figure 4 are from the circuit shown in Figure 5. For such an application, the most challenging part is how to ensure that the DC voltage across each stage in Figure 4 is maintained nearly the same. Circuit topology in Figure 5 is potentially a choice. One DC microgrid is designed to supply power to one inverter and different inverters have separate DC microgrids to supply power. To make the voltage at each stage of each phase nearly the same in an inverter, it is necessary 1) to keep the voltage at DC microgrid to fluctuate very slightly; 2) to keep the voltage drop as small as possible across the DC/AC inverter, medium-frequency transformer, AC/DC rectifier at different loading levels and also to keep contact resistances as small as possible in Figure 5. The circuit shown in Figure 4 can be used to form the grid-forming, grid-supporting and grid-feeding generators in a microgrid. To operate the system stably, it is better to have small variation of loads' demand. Then gradual changes of generations from the generators can cope with it. The grid-forming generator can choose to operate at nearly constant power transferring. Such a microgrid, named as the upstream large-scale microgrid, is to supply power to downstream three-phase or equivalent three-phase loads through step-down transformers or multiple downstream microgrids operated at constant frequency, each of which is interfaced with the upstream large-scale microgrid through single back-to-back converter for a small downstream microgrid or multiple solid-state transformers in parallel for a relatively large downstream microgrid. The power transferred through them to downstream microgrids in one-direction is fixed or only experiences ramping change from one to another level. To alleviate the influence by the distributed capacitors along transmission lines, a wye-delta connected transformer either step-up or step-down needs to be used with each of generators formed by the circuit in Figure 4.

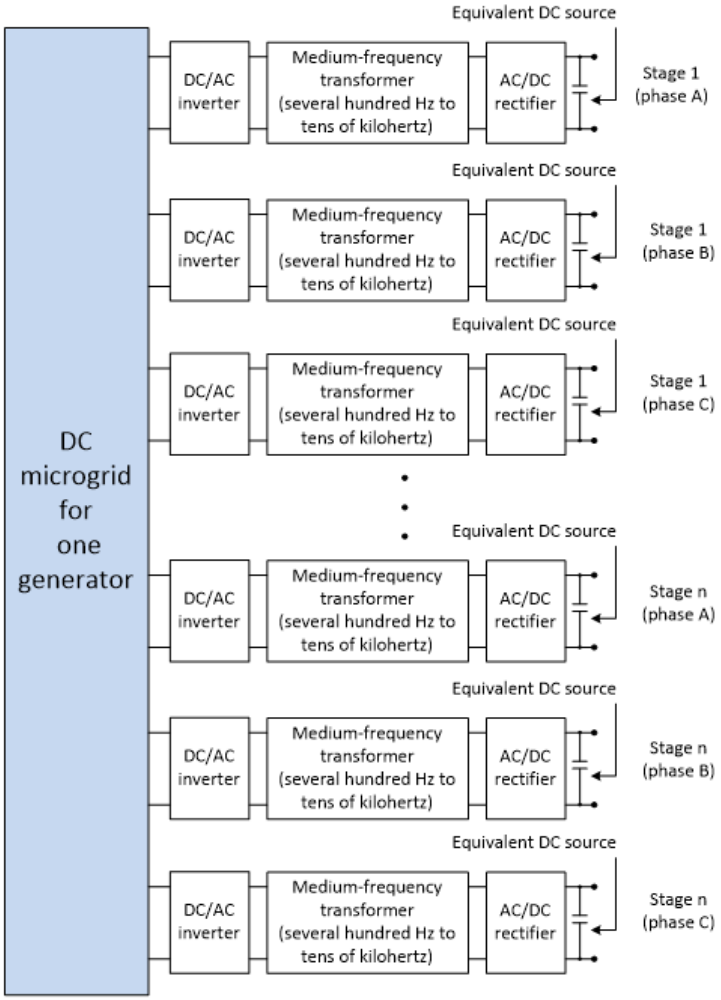

Figure 5 Equivalent DC source for each stage in the circuit shown in Figure 4.

The multi-stage topology in Figure 4 contains many components. Failure of one component results in the whole inverter to fail to operate. Rationally, it could be better to use conventional synchronous generator or other stable sources to supply power to one-stage LCCL filtered back-to-back converter to serve as the grid-forming generator [21]. This is because it contains far less components, yet still can handle relatively high power. The back-up grid-forming generator could be formed in the same approach. Several, instead of one one-stage LCL filtered converters can be adopted for reactive power compensation installed with the grid-forming generator. Nevertheless, with partly moulded design of the circuit in Figure 4 to construct the grid-forming generator and its back-up one, the system will have higher reliability. Then grid-feeding generators formed by the solar energy and wind energy harnessing and even energy from storage can be tapped into the microgrid directly using the topologies in [11] together with 50Hz transformers.

Besides three-phase autonomous microgrid operated at constant frequency, one can adopt single-phase microgrids operated at constant frequency as described in [9, 21] using one-stage or multi-stage circuits of one phase circuit from Figure 4. The step-down transformer is necessary to supply power to single-phase loads when the inverters operate at high voltage.

4. Conclusions

This paper presents a new small-signal analysis on the autonomous microgrid operated at constant frequency. It builds the difference equation for the reactive power of the grid-forming generator based on reactive power balance in the overall system. For the voltage source inverter with its current controlled by proportional resonant controller, at the fundamental frequency, its output current is disentangled from its terminal voltage and is controlled to trace its reference accurately, namely $i_{out} = i_{out}^{*}$. Therefore, each inverter can be modelled as an equivalent current source and the equivalent circuits for d-component and q-component can be separated from each other. Then, the nodal equations in matrix form for the microgrid system can be established readily and the system level state-space equation has been constructed. Steady-state d-q values of voltage and currents at each bus are adopted in calculating the eigenvalues of the system matrix. It is found that the selected coefficients for real power and reactive power reference generation and controller's parameters can make the eigenvalues fall in the left-half side of a complex plane and the system is stable. This is in agreement with the time-step modelling of the system in Matlab/Simulink. Such a research paves the way for further working out the safe operation region with sufficient margin from unstable boundary.

Author Contributions

The authors did all the research work of this study.

Competing Interests

The authors have declared that no competing interests exist.

References

1. Zhong QC. Robust droop controller for accurate proportional load sharing among inverters operated in parallel. IEEE Trans Ind Electron. 2011; 60: 1281-1290.
2. Zhang Z, Huang X, Jiang J, Wu B. A load-sharing control scheme for a microgrid with a fixed frequency inverter. Electr Power Syst Res. 2010; 80: 311-317.
3. Olivares DE, Mehrizi Sani A, Etemadi AH, Cañizares CA, Iravani R, Kazerani M, et al. Trends in microgrid control. IEEE Trans Smart Grid. 2014; 5: 1905-1919.
4. De Brabandere K, Bolsens B, Van den Keybus J, Woyte A, Driesen J, Belmans R. A voltage and frequency droop control method for parallel inverters. IEEE Trans Power Electron. 2007; 22: 1107-1115.
5. Guerrero JM, Matas J, de Vicuna LG, Castilla M, Miret J. Decentralized control for parallel operation of distributed generation inverters using resistive output impedance. IEEE Trans Ind Electron. 2007; 54: 994-1004.
6. Mohamed YA, El-Saadany EF. Adaptive decentralized droop controller to preserve power sharing stability of paralleled inverters in distributed generation microgrids. IEEE Trans Power Electron. 2008; 23: 2806-2816.
7. Teodorescu R, Liserre M, Rodriguez P. Grid converters for photovoltaic and wind power systems. Hoboken, NJ, US: John Wiley & Sons; 2011.

8. Zhang D. Operation of microgrid at constant frequency with a standby backup grid-forming generator. Proceedings of the 2016 IEEE International Conference on Power System Technology; 2016 September 28; Wollongong, NSW, Australia. New York, NY, US: IEEE.
9. Zhang D, Fletcher J. Design and operation of an islanded microgrid at constant frequency. In: Development and Integration of Microgrids. London, UK: IntechOpen; 2017.
10. Zhang D. Operation of AC microgrids with PV panels' output power curtailment for minimizing the use of energy storage. J Energy Power Technol. 2022; 4: 008.
11. Zhang D. Modeling of autonomous microgrid operated at medium-voltage level and at constant frequency and study of its voltage profile. J Energy Power Technol. 2023; 5: 009.
12. Rommes J, Martins N. Computing large-scale system eigenvalues most sensitive to parameter changes, with applications to power system small-signal stability. IEEE Trans Power Syst. 2008; 23: 434-442.
13. Coelho EA, Cortizo PC, Garcia PF. Small-signal stability for parallel-connected inverters in stand-alone AC supply systems. IEEE Trans Ind Appl. 2002; 38: 533-542.
14. Godoy RB, Pinto JO, Canesin CA, Coelho EA, Pinto AM. Differential-evolution-based optimization of the dynamic response for parallel operation of inverters with no controller interconnection. IEEE Trans Ind Electron. 2012; 59: 2859-2866.
15. Kahrobaeian A, Mohamed YA. Analysis and mitigation of low-frequency instabilities in autonomous medium-voltage converter-based microgrids with dynamic loads. IEEE Trans Ind Electron. 2013; 61: 1643-1658.
16. Hassan MA, Abido MA. Optimal design of microgrids in autonomous and grid-connected modes using particle swarm optimization. IEEE Trans Power Electron. 2010; 26: 755-769.
17. Tang X, Zhang D. Islanded AC microgrid stability and feasibility analysis on V-P control with estimation at constant frequency. Proceedings of the 2019 9th International Conference on Power and Energy Systems; 2019 December 10; Perth, WA, Australia. New York, NY, US: IEEE.
18. Khalid HM, Peng JC. Tracking electromechanical oscillations: An enhanced maximum-likelihood based approach. IEEE Trans Power Syst. 2015; 31: 1799-1808.
19. Khalid HM, Peng JC. Improved recursive electromechanical oscillations monitoring scheme: A novel distributed approach. IEEE Trans Power Syst. 2015; 30: 680-688.
20. Zhang D. Issues on autonomous ac microgrid operated at constant frequency. In: 2021 31st Australasian Universities Power Engineering Conference (AUPEC). New York, NY, US: IEEE; 2021. pp. 1-7.
21. Zhang D. Circuits of voltage source dc/ac converter with LCCL or LCC filter and other modified forms, and operation of microgrid with such circuits. 2017. Available from: https://patents.google.com/patent/WO2017106902A1/zh.